CAMBRIDGE
UNIVERSITY PRESS

Article

Adsorption of gold nanoparticles on illite under high solid/liquid ratio and initial pH conditions

Ping Zeng[1,2], Xin Nie[1], Zonghua Qin[1], Suxing Luo[3], Yuhong Fu[4], Wenbin Yu[1], Meizhi Yang[5], Wenqi Luo[1,2], Hai Yang[6] and Quan Wan[1,7]

[1]State Key Laboratory of Ore Deposit Geochemistry, Institute of Geochemistry, Chinese Academy of Sciences, Guiyang, Guizhou, China; [2]University of Chinese Academy of Sciences, Beijing, China; [3]Department of Chemistry and Chemical Engineering, Zunyi Normal College, Zunyi, China; [4]School of Geographic and Environmental Sciences, Guizhou Normal University, Guiyang, China; [5]Office of Academic Research, Guizhou Open University, Guiyang, China; [6]Hunan Provincial Key Laboratory of Environmental Catalysis and Waste Recycling, School of Chemistry and Chemical Engineering, Hunan Institute of Engineering, Xiangtan, China and [7]CAS Center for Excellence in Comparative Planetology, Hefei, China

Abstract

Adsorption of nanoparticles on minerals affects the fate and transport of nanoparticles directly and is of great significance to many fields, including research into ore deposits, geochemistry, the environment and mineral materials. Whereas many previous studies have been conducted under the equilibrium pH and low solid (mineral) to liquid (nanoparticle suspension) ratio conditions, adsorption processes under initial pH and high solid/liquid ratio conditions may represent many important yet underexamined complex scenarios. To fill in this research gap, the adsorption of gold nanoparticles on illite was investigated experimentally at a relatively high solid/liquid ratio of 5 g L^{-1} and the effects of initial pH, ionic strength, citrate concentration, temperature and illite particle size were evaluated. The adsorbed amount of gold nanoparticles (from <5% to nearly 100%) increased with increasing ionic strength, temperature and citrate concentration and decreased with increasing pH and illite particle size. The presence of illite resulted in the dynamic evolution of the pH of the suspension, which, along with solution chemistry parameters, controlled the electrostatic interaction of illite and gold nanoparticles. The adsorption results, scanning electron microscopy observations and surface properties of illite suggest that the negatively charged gold nanoparticles were adsorbed predominantly on the positive illite edges through electrostatic interaction. The electrostatic attraction between illite and gold nanoparticles appeared to be strong, supported by the minor amount of desorption. These research findings are expected to provide a valuable reference regarding many critical issues in the geosciences as well as for industrial applications.

During the last several decades, large quantities of engineered nanoparticles (ENPs) have been manufactured owing to their size-dependent properties and numerous applications in consumer and industrial products (Hendren *et al.*, 2011; Sharma *et al.*, 2019; Abbas *et al.*, 2020a), and hence the potential release of ENPs into the land, soil, water, air and ecosystems and the associated impacts of this have attracted considerable attention (Nowack & Bucheli, 2007; Brar *et al.*, 2010; Keller *et al.*, 2013). Since Earth's origin, natural nanoparticles (NNPs) formed *via* various natural processes have been abundantly present, with the estimated annual flux of NNPs (hundreds of teragrams) to the Earth's surface and atmosphere being around three orders of magnitude greater than that of ENPs (Hochella *et al.*, 2019). Given the distinctive behaviours of natural and anthropogenic nanoparticles (NPs) as well as their abundance and ubiquity in the Earth system, it has become increasingly recognized that NPs might play critical yet not entirely understood roles in many Earth processes, with

fundamental implications possibly traversing multiple temporal and spatial scales (Hochella *et al.*, 2002, 2008, 2019).

One of the most relevant such research topics addresses the interaction of NPs with their surrounding minerals in natural environmental media, specifically the adsorption of NPs on minerals (or heteroaggregation between NPs and minerals). As indicated by numerous previous studies, because the transport, exposure route, fate, distribution and bioavailability of NPs can all be substantially influenced by the adsorption of NPs on minerals, understanding such adsorption behaviour is desirable in various scientific fields, including but not limited to ore deposit formation (Reich *et al.*, 2005; Hannington *et al.*, 2016; Zhou *et al.*, 2017), explorative geochemistry (Cao & Cheng, 2020; Hu *et al.*, 2020), environmental science (Novikov *et al.*, 2006; Sharma *et al.*, 2015; Hochella *et al.*, 2019), ecology (Buzea *et al.*, 2007; Hochella *et al.*, 2008; Wang *et al.*, 2019), nanotoxicity (Borm *et al.*, 2006; Amde *et al.*, 2017; Abbas *et al.*, 2020b), catalysis (Bond & Thompson, 2006; Wang *et al.*, 2014) and analytical science (Alvarez-Puebla *et al.*, 2005; Sathuluri *et al.*, 2011; de Barros *et al.*, 2017). For example, in the field of ore deposits, the transport and adsorption of metallic NPs on host minerals has long been proposed as an effective metal enrichment

mechanism for several important hydrothermal and supergene deposits (Frondel, 1938; King *et al.*, 2014; Saunders & Burke, 2017; Petrella *et al.*, 2020, 2022; Saunders *et al.*, 2020; McLeish *et al.*, 2021; Wierchowiec *et al.*, 2021), whereas the geochemical anomalies detected in the overburden and that are useful in locating buried economic mineral deposits can result from the natural dispersion of indicator element-bearing NPs and therefore should be influenced by the adsorption/deposition of NPs (Wang *et al.*, 2016; Reith & Cornelis, 2017; Zhang *et al.*, 2019). In environmental science, an ongoing concern is how and to what extent nanotechnology will impact the environment, organisms and human health, and various transformations of NPs (especially ENPs), including adsorption, agglomeration and chemical reactions in various environment compartments, have been demonstrated to change significantly their mobility, exposure form, bioavailability and toxicity (Tiede *et al.*, 2009; Wang *et al.*, 2019; Abbas *et al.*, 2020a, 2020b; Spurgeon *et al.*, 2020).

To date, several investigations have been performed to understand the adsorption behaviour of NPs (metals, metal oxides, graphene oxides, etc.) on minerals (pyrite, goethite, quartz, montmorillonite, kaolinite, diatomite, etc.), unveiling a complex adsorption process coregulated by a variety of factors including the physicochemical characteristics of NPs/minerals (composition, structure, morphology, surface charge, etc.) and solution conditions (pH, ionic strength (IS), electrolyte, organic matter, temperature, etc.) (Mikhlin *et al.*, 2007; Zhou *et al.*, 2012; Labille *et al.*, 2015; Wang *et al.*, 2015b, 2019; Zhao *et al.*, 2015; Fu *et al.*, 2017; Luo *et al.*, 2018; Syngouna *et al.*, 2018; Lu *et al.*, 2019; Dong & Zhou, 2020; Li *et al.*, 2020). By combining the effects of van der Waals attraction, electric double-layer (EDL) forces and perhaps additional interactions, the classical and extended Derjaguin–Landau–Verwey–Overbeek (DLVO) theories serve well as useful frameworks to account for observed aggregation and adsorption behaviours between colloidal particles, at least in a semiquantitative manner (Derjaguin & Landau, 1941; Verwey & Overbeek, 1948; Thio *et al.*, 2010; Wang *et al.*, 2015a). Yet the quantitative explanation and prediction of such behaviours are still lacking (Hotze *et al.*, 2010; Petosa *et al.*, 2010; Liu *et al.*, 2013, 2014), and sometimes the discrepancies between theories and observations can reach several orders of magnitude (Elimelech *et al.*, 1995; Petosa *et al.*, 2010). Such serious disparities, which can be attributed to the challenges stemming from the small size and special structure of NPs and the surface charge heterogeneities of minerals, not only demonstrate the inadequacy of the DLVO theories to quantify NP–mineral interactions accurately, but also warrant experimental endeavours to gather basic adsorption data.

Analytical approaches of counting and sizing NPs, such as dynamic light scattering (DLS) and time-resolved laser diffraction, have often been employed to acquire valuable information on aggregation rate and attachment efficiency. Despite the proven potency of such methodologies in heteroaggregation studies, their general limitation to dilute suspensions and intrinsic overestimation of larger-sized mineral particles cannot be overlooked (Zhou *et al.*, 2012; Labille *et al.*, 2015; Liu *et al.*, 2015; Wang *et al.*, 2015b, 2019; Gallego-Urrea *et al.*, 2016; Praetorius *et al.*, 2020). Although many laboratory experiments have been carried out successfully under pre-adjusted pH conditions to obtain equilibrium adsorption results (Labille *et al.*, 2015; Liu *et al.*, 2015; Wang *et al.*, 2015b, 2019, 2021; Huang *et al.*, 2016; Syngouna *et al.*, 2018; Tang & Cheng, 2018; Lu *et al.*, 2019; Dong & Zhou, 2020; Guo *et al.*, 2020), we argue that such pre-adjustment

of pH is not a necessary step in many important natural and even some engineering processes. Instead, real-world scenarios often involve interaction (or mixing) between a substantial amount of minerals (high solid/liquid ratio) and a NP-containing fluid with an initial pH. For example, as mentioned earlier, the interaction of a metallic NP-bearing fluid (having an initial pH) with wall rock may be critical to the formation of certain ore deposits (e.g. Carlin-type gold deposits), while the rock/fluid ratio can be as high as 5 g L^{-1} (Kusebauch *et al.*, 2018; Kusebauch *et al.*, 2019). The suspended particulate matter (SPM) of some rivers, into which release of ENPs is possible, can reach up to tens of grams per litre (e.g. during floods; Thill *et al.*, 2001; Slomberg *et al.*, 2017). In sewage treatment plants, activated sludge is used to remove NPs from wastewater at a solid/liquid ratio of a few grams per litre (Barton *et al.*, 2014; Chen *et al.*, 2014), whereas in soil remediation sites, NPs are used to remediate contaminated soil at a solid/liquid ratio of hundreds of grams per litre (Machado *et al.*, 2013; Zialame *et al.*, 2021). It should be noted that dynamic evolution from initial to final pH of the mixed suspensions is expected in most of the above cases due to reactions between protons and minerals, especially at high solid/liquid ratios.

To the best of our knowledge, there are very few systematic investigations of the adsorption of NPs on minerals under conditions of a high solid/liquid ratio and an initial pH, which may simulate accurately several important processes and applications. Therefore, in this work, we carried out an experimental study of gold NP (AuNP) adsorption with illite under the conditions of a relatively high solid/liquid ratio (5 g L^{-1}) and initial pH values of 4–10. AuNPs were chosen as representative metallic NPs mainly because of their confirmed occurrences and potentially important roles in a number of ore deposits (e.g. at the rim of clay mineral grains in weathering deposits) and in some surficial environments (Bakken *et al.*, 1989; Hong *et al.*, 1999; Palenik *et al.*, 2004; Reich *et al.*, 2005; Hough *et al.*, 2008, 2011; Southam *et al.*, 2009; Lintern *et al.*, 2013; Saunders & Burke, 2017; Zhou *et al.*, 2017; Wierchowiec *et al.*, 2021). Clay minerals are important components of sediments and soils that are distributed widely in supergene environments and critical zones (Bergaya & Lagaly, 2013; Hochella *et al.*, 2019), and they show great potential in agricultural, industrial and medicinal applications (Bedelean *et al.*, 2009; Floody *et al.*, 2009; Martin *et al.*, 2018). As one of the most common and major potassium clay minerals in the surface environment, illite (a dioctahedral 2:1 phyllosilicate) accounts for more than half of the total clay minerals in the Earth's crust (Gradusov, 1974). We thus selected illite to represent the widespread clay minerals in the environment, which, given their ubiquity, are very likely to interact with NPs and affect the fate and transport of NPs significantly (Zhou *et al.*, 2012; Sotirelis & Chrysikopoulos, 2016; Yu *et al.*, 2019, 2020). Furthermore, the patch-wise charge heterogeneity and great specific surface area of clay minerals may have a profound influence on the adsorption behaviour of AuNPs. To the best of our knowledge, only a few experimental studies have been reported on the adsorption of AuNPs on clay minerals. Among them, Gallegot-Urrea *et al.* (2016) tested the aggregation rate of AuNPs (80 μg L^{-1}) under simulated natural freshwater conditions using DLS. Possibly due to the relatively low concentration of illite (650 μg L^{-1}), illite did not promote the agglomeration of AuNPs significantly (Gallego-Urrea *et al.*, 2016). By evaluating the distribution and adsorption behaviour of AuNPs in soil, Reith *et al.* (2017) found that clay minerals and organic matter in soil were

the most important adsorbents of AuNPs. Yet the influence of the medium conditions on the adsorption of AuNPs by a single adsorbing component (e.g. a clay mineral) in the soil was not investigated specifically (Reith *et al.*, 2017). Our experimental investigation of AuNP adsorption on illite under various solution conditions has generated systematic data and findings that we believe will provide new insights into the governing mechanisms of AuNP–illite adsorption and shed light on the role of NPs in aquatic environments.

Materials and methods

Reagents

Chloroauric acid tetrahydrate (HAuCl$_4$·4H$_2$O; ≥99.9%) was purchased from Shanghai Jiuyue Chemical Corporation (Shanghai, China). Trisodium citrate (≥99.9%) was purchased from Shanghai Shenbo Chemical Corporation (Shanghai, China). Hydrochloric acid (HCl; 36–38%), nitric acid (HNO$_3$; 65–68%), sodium chloride (NaCl; ≥99.0%) and sodium hydroxide (NaOH; 99.0%) were purchased from Sinopharm Chemical Reagent Corporation (Shanghai, China). All solutions were prepared using deionized water (Millipore Corporation, Molsheim, France) with a specific resistivity of 18.2 MΩ·cm. All glassware was cleaned and soaked in aqua regia (HCl/HNO$_3$ = 3:1, v/v) for at least 8 h, before a thorough rinse with deionized water followed by oven drying at 50°C for 48 h.

Synthesis and characterization of AuNPs

Monodisperse suspensions of negatively charged AuNPs with a particle size of ~18 nm were synthesized using the Frens method (Frens, 1973), in which sodium citrate was used as a reducing agent and stabilizer. Briefly, 300 mL of HAuCl$_4$ solution (0.01%, w/w) was first heated to boiling. Then, 10.5 mL of sodium citrate solution (1.00%, w/w) was added rapidly, and the boiling was continued for 20–30 min to complete the reaction. After the reaction, a wine-red suspension of AuNPs was obtained, which was cooled to room temperature and then stored in a refrigerator at 4°C. The Au concentration of the as-synthesized suspension measured using atomic absorption spectroscopy (AAS; 990SUPER, Persee, Beijing, China) was ~57.6 ppm. The particle size and ζ-potential of AuNPs were determined using a multi-angle particle sizer and high-sensitivity ζ-potential analyser (Omni, Brookhaven Instruments, New York, NY, USA), respectively. Only negligible changes in particle size and ζ-potential (Fig. S1) were found after 5 days of storage (greater than the adsorption period), indicating that our AuNP suspensions were relatively stable.

Illite sample characterization

The illite sample was collected from Jinsha, Guizhou Province, China. A fraction of illite particles <2 μm was obtained through washing, crushing, milling and sedimentation. The crystal structure of illite was verified using power X-ray diffraction (XRD; Empyrean, Eindhoven, The Netherlands) analysis, which was conducted with Cu-*K*α radiation operated at 40 kV and 40 mA, and with a scan of 5°–60°2θ (Fig. S2a). The major element composition was determined using X-ray fluorescence (XRF; ARL Perform'X 4200, Thermo Fisher, Waltham, MA, USA) spectrometry (Table S1). Because of the similar XRD features of illite and muscovite, thermal analysis (STA 449 F3 Jupiter, Selb, Germany) and XRF were used to distinguish the two minerals. In comparison with muscovite, the lower dehydroxylation temperature (Fig. S2b), lesser potassium content (Table S1) and the XRD analysis results confirmed that our sample was high-purity illite (Gaines *et al.*, 1964; Mackenzie *et al.*, 1966; Schomburg *et al.*, 1997). The typical scale-like surface morphology of the illite sample was characterized using scanning electronic microscopy (SEM; Scios, Hillsboro, OR, USA; Fig. S3) with an acceleration voltage of 30 kV. The electrokinetic potential and the point of zero charge (pH$_{PZC}$; ~5.8) of the illite sample were determined using a ζ-potential analyser (Omni, Brookhaven Instruments, New York, NY, USA) and an automatic potentiometric titrator (Metrohm 905, Herisau, Switzerland), respectively (Fig. S4).

Batch adsorption experiments

Batch adsorption experiments were conducted under controlled solution chemistry conditions to examine the effects of pH, IS, natural organic matter (NOM) and temperature on the adsorption behaviour of AuNPs on illite at a constant solid/liquid ratio of 5 g L^{-1}. All batch experiments were performed in a constant-temperature shaker and were run at least in duplicate. The initial pH of each AuNP suspensions was adjusted in the range of 4–10 using 2 M HCl or NaOH solution. The concentration of sodium citrate in AuNPs suspensions was varied in the range of 1.0–7.5 mM to investigate its effect on adsorption behaviour, with the background concentration of sodium citrate from the as-synthesized AuNP suspension determined to be ~1 mM. The ISs of the Au colloids were controlled by adding various amounts (0, 5 or 10 mM) of NaCl to the suspensions. For a typical adsorption experiment, 0.2 g of illite and 40 mL of 57.6 ppm AuNP suspension were added into a 100 mL conical flask and shaken for 5 days at various temperatures (5, 25 or 60°C). Subsequently, 3–5 mL of the mixed suspension was sampled and centrifuged for 30 min (3000 rpm). Then, 1 mL of the supernatant was collected and digested (1 mL aqua regia, overnight) to analyse the Au concentration using AAS. The sodium citrate concentrations of the suspensions before and after adsorption were determined using high-performance liquid chromatography (HPLC; Agilent 1200, Santa Clara, CA, USA). The ζ-potential and dissolved cation concentrations of illite under various solution chemistry conditions were determined using a ζ-potential analyser (Omni, Brookhaven Instruments, New York, NY, USA) and inductively coupled plasma optical emission spectrometry (ICP-OES; VISTA-MPX, Varian, Palo Alto, CA, USA), respectively. All of the tests were performed at least in duplicate. Based on the measured concentration of Au or sodium citrate, the adsorption amount (q_t) and adsorption percentage (%R) were calculated according to Equations 1 and 2:

$$q_t = Vc_0(1 - \frac{C}{C_0})/m \tag{1}$$

$$\%R = (1 - \frac{C}{C_0}) \times 100\% \tag{2}$$

where c is the concentration of the supernatant at time t, c_0 is the initial concentration of the solution, $\frac{C}{C_0}$ is the relative residual (unadsorbed) concentration of Au or sodium citrate in the supernatant, V is the volume of the solution and m is the mass of the illite sample.

The desorption experiments were conducted by first separating illite (centrifugation: 3000 rpm, 30 min) from the sorption suspensions and then shaking it in 40 mL of deionized water or 1 mM sodium citrate solution (similar to the background concentration in the as-synthesized AuNP suspension) at pH 4. As with the adsorption experiments, after desorption, the concentration of Au in the supernatant was measured using AAS.

Results and discussion

Effect of pH on the adsorption of AuNPs on illite

As the surface electrical properties of both AuNPs and illite will change with varying pH (Cottet *et al.*, 2014; Rawat *et al.*, 2018), the adsorption behaviour of AuNPs with pH as a master variable was first investigated. The initial pH range of AuNP suspensions was chosen to be 4–10, which is close to the pH range of natural water (Huertas *et al.*, 2001). As indicated in Fig. S1, within the whole experimental pH range, all of our AuNPs were negatively charged (due to complexation with negatively charged citrate groups) and all suspensions remained stable for over 5 days. For illite as a typical 2:1 clay mineral, the substitution of Si^{4+} and Al^{3+} in the tetrahedral and octahedral sheets by lower-valence cations creates permanent negative charges on the basal planes, whereas pH-dependent charges develop at the edges of the illite planes where the Si–Al lamellar structure breaks (Avena, 2003; Delhorme *et al.*, 2010; Liu *et al.*, 2013). At pH values below the pH_{PZC} (measured to be 5.8), the basal plane of illite is negatively charged, whereas the illite edge is positively charged due to the protonation of the amphoteric Si–OH and Al–OH groups. At pH values greater than the pH_{PZC}, both the illite edge and basal plane are negatively charged. It is worth noting that at a relatively high solid/liquid ratio (5 g L^{-1}), a change in the system pH was anticipated due to the interlayer cation exchange of illite and the protonation or deprotonation of the hydroxyl groups on the edge face of illite. As shown in Fig. S5, when the initial pH was changed from 4 to 7, the suspension pH eventually rose from 4.9 to 8.1, and the decrease of pH from 10.0 to 8.4 was due to the influence of atmospheric carbon dioxide.

Figure 1a shows the relative concentrations of AuNPs in the supernatant as a function of adsorption time and initial pH. It can be seen that all adsorption experiments at various initial pH values almost attained equilibrium when the adsorption time reached ~30 h, and the adsorption amount decreased with increasing pH. The maximal adsorption (~70%) of AuNPs on illite occurred at the lowest initial pH of 4. At pH > 5, only <10% of AuNPs were adsorbed on illite after 50 h of adsorption, whereas insignificant adsorption of AuNPs was observed at a pH > 7. Such adsorption behaviour is explained through electrostatic interaction between the negative charge of AuNPs and the patch-wise charge on illite. At pH < pH_{PZC} of illite, although the overall electrical interaction between AuNPs and illite (due to its dominant negative charge at basal planes; see Fig. S4a) is still repulsive, the positive charges (i.e. protonated hydroxyl groups) on illite edges provide attractive adsorption sites for negatively charged AuNPs (see Fig. S1a). More importantly, our experiments imply that when AuNPs migrated to the vicinity of the illite edge and possibly with a proper orientation, the repulsion between AuNPs and illite can be overcome and the resulting local net attraction can lead to the favourable adsorption of AuNPs. The adsorption amount would depend on both the repulsive and attractive forces between AuNPs and the heterogeneous structure

of illite. Thus, the greatest adsorption took place at pH 4 (among the pH range of 4–10), when the repulsion appeared to be the least (due to lower absolute ζ-potential values for both AuNPs and illite; see Figs S1a & 4a) and the attraction might be greatest (due to greater positive charge at the illite edge; see Fig. S4b). Similarly, when pH increased, the repulsion became stronger while the attraction diminished gradually, leading to a lesser adsorption extent. Finally, when the system pH (e.g. initial pH 7–10) was significantly greater than the pH_{PZC} of illite, the attraction force for AuNPs at the negatively charged illite edge disappeared, and then the AuNPs adsorption became negligible.

The adsorption behaviour of citrate alone (c_0: 1 mM, similar to the concentration of the as-synthesized AuNP suspension) on illite was further compared as a function of adsorption time and pH. Figure 1b shows that the adsorption amount of citrate on illite decreased with increasing pH, consistent with the adsorption trend of AuNPs. As citric acid is a triprotic carboxylic acid, the citrate molecule was always negatively charged under our experimental conditions, and its speciation and average charge depended on the pH of the solution. In general, the adsorption behaviour of organic acids can be explained by considering the electrostatic interactions between the carboxylic acid species and the charged surface sites of clay minerals (Ward & Brady, 1998). Similar to the AuNP adsorption mechanism discussed above, a greater pH induces greater repulsion and less attraction between citrate (with more deprotonated species; Ramos & Huertas, 2014) and illite (with diminishing positive charges at edge faces), resulting in a reduced adsorption amount of citrate at greater pH values. Such a similar adsorption trend with pH confirms the importance of citrate dissociation on the surface of AuNPs as well as the heterogeneous charging behaviour of illite, therefore reinforcing the related electrostatic mechanism in the adsorption process. Despite the apparent resemblance between AuNP and citrate adsorptions on illite, the percentage adsorption of AuNPs is generally lower than that of citrate (Fig. 1c), which is attributed to the greater repulsion between illite and AuNPs complexed with many citrate surface ligands. As the maximum adsorption amount of AuNPs on illite occurred at pH 4, we will set the initial pH of the suspension to 4 to illustrate the influences of IS, sodium citrate concentration and temperature on the adsorption process in the following sections.

Effect of IS on the adsorption behaviour of AuNPs

IS is known to affect the electrostatic potential of charged particles such as NPs and clay minerals and thus to affect their aggregation and adsorption behaviours (Rawat *et al.*, 2018). Generally, an increase in the solution IS leads to a decrease in both the range and magnitude of the EDL interactions. To elucidate the effect of IS on the adsorption process, we conducted adsorption experiments with controlled IS (through the addition of 0, 5 or 10 mM NaCl) at pH 4 and at a constant solid/liquid ratio of 5 g L^{-1}. As shown in Fig. 2a, the adsorption rate and adsorption amount of AuNPs on illite increased significantly with the addition of NaCl, in agreement with the similar impact of ζ-potential found in previous studies (Saka *et al.*, 2006; Lu *et al.*, 2019). At a concentration of 10 mM added NaCl, ~94% of AuNPs were removed from the suspension within just 0.5 h. Such a sharp influence of IS on the adsorption process can be explained in terms of the following aspects: first, in consideration of the patch-wise charge heterogeneity of illite, the spillover of the illite basal plane EDL to the edge is substantial at low IS and will to some
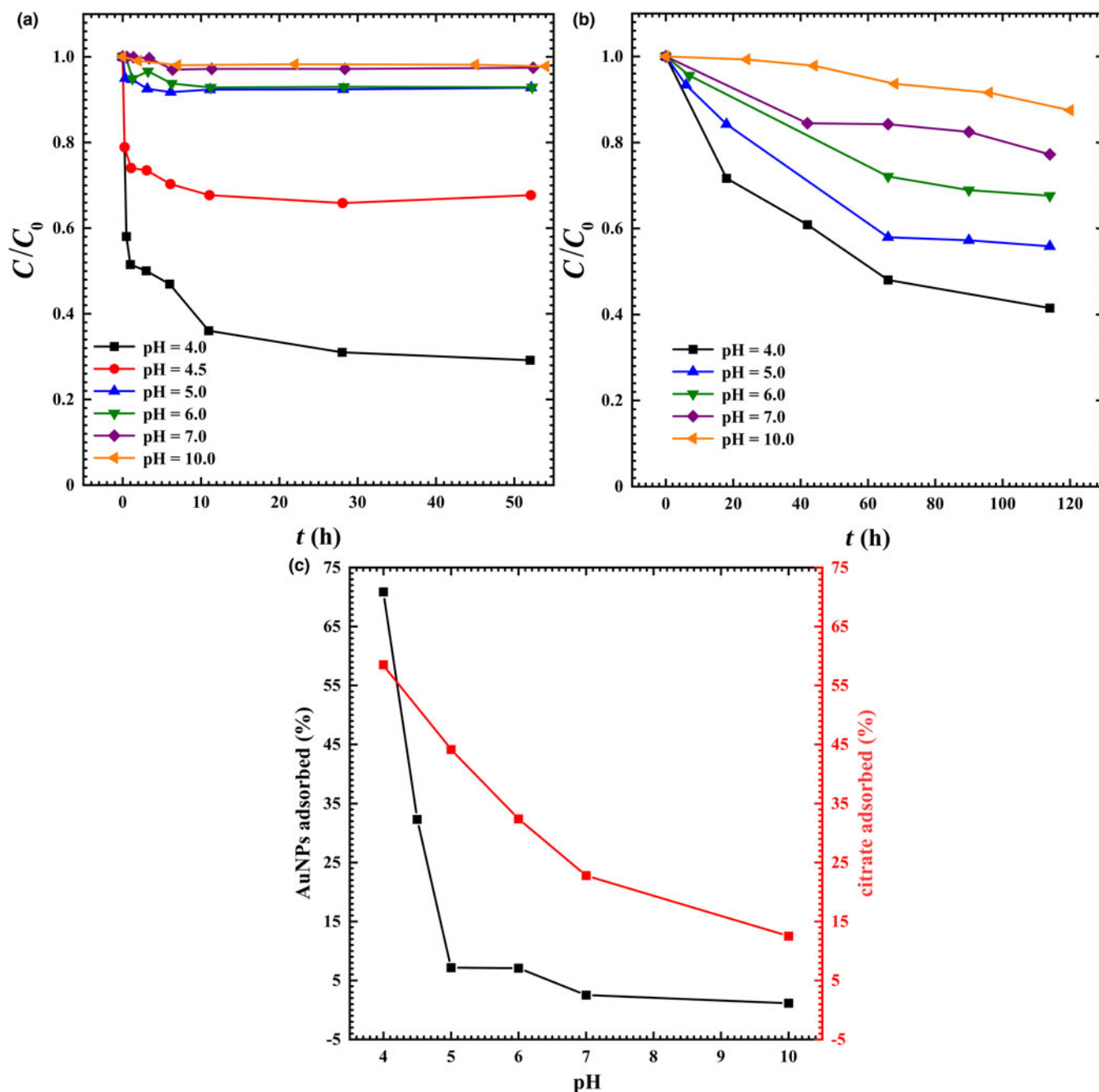
Figure 1. (a) Relative residual concentration of AuNPs in the supernatant at various initial pH values as a function of adsorption time. (b) Relative residual concentration of citrate in the supernatant at various initial pH values as a function of pH adsorption time. (c) Adsorbed AuNPs and citrate on illite at various initial pH values.

extent shield the edge EDL, thus creating a strong repulsive energy barrier to the approaching AuNPs. At an increased IS, the EDL on the basal plane becomes sufficiently compressed (Fig. 2b) and therefore the attractive EDL on the edge will emerge as a more influential force for the adsorption of more AuNPs (Tombácz & Szekeres, 2004; Zhou *et al.*, 2012). Second, an increase in IS also screens the electrostatic repulsions amongst charged AuNPs, making them less stable and more prone to homoaggregation. Such a promoted homoaggregation of AuNPs by increased IS was also observed in our previous investigations (Luo *et al.*, 2018).

Effect of citrate concentration on AuNP adsorption

As discussed above, citrate exists as a surface ligand that stabilizes AuNPs, and its concentration in our as-synthesized suspension was ~1 mM. As a low-molecular-weight organic anion, citrate has been found in natural environments, including soil, sediments and aerosols, and it can originate from the metabolic processes of plant roots and microorganisms (Ryan *et al.*, 2001; Braissant *et al.*, 2002). In addition, citrate is often used as a reducing and stabilizing agent in the process of ENP synthesis, and it can be released with ENPs and influence on ENP transformations
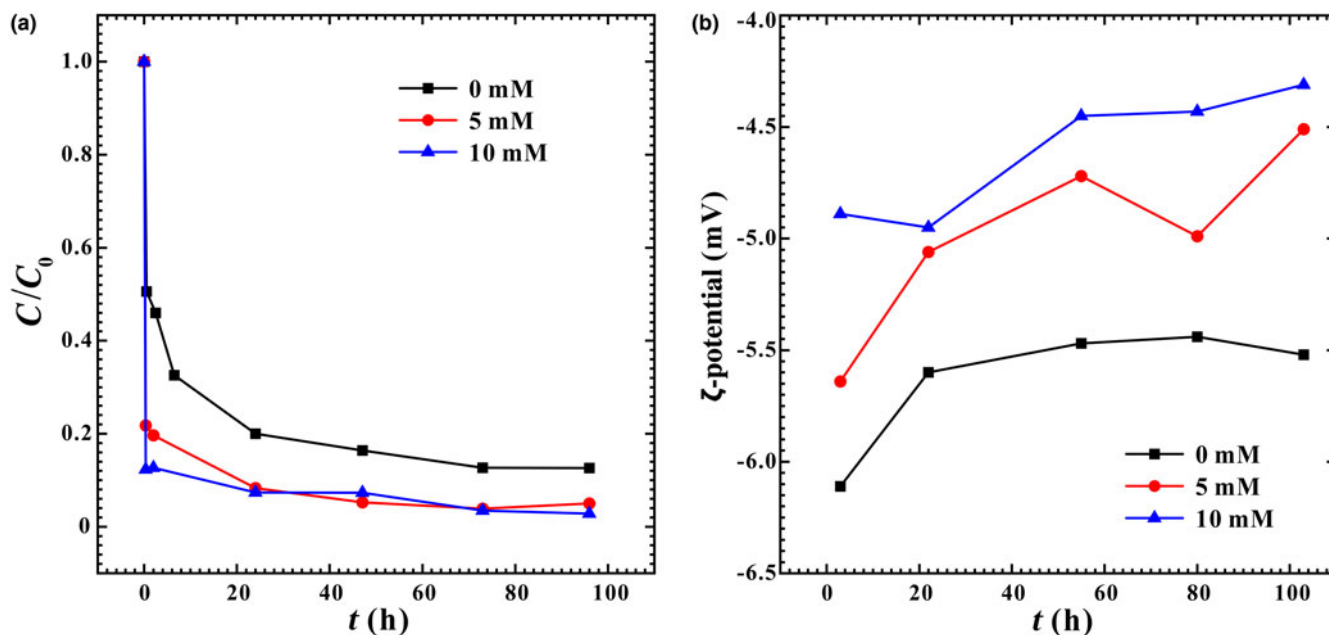
Figure 2. (a) Effect of IS (addition of 0, 5 or 10 mM NaCl) on the adsorption of AuNPs on illite. (b) ζ-potential of illite under various IS conditions.

(Wagener *et al.*, 2012). Therefore, there is a need to explore the effects of citrate as a representative organic compound on the adsorption of AuNPs on illite. For organic molecules in NP suspensions, both stabilization (due to electrosteric forces) and destabilization (due to bridging) roles have been recorded experimentally, and it is often difficult to predict these interactions (Wang *et al.*, 2015a; Gallego-Urrea *et al.*, 2016; Tang *et al.*, 2018; Ahmed *et al.*, 2021). Compared with many other natural organic compounds, such as humic acid, citrate has the advantages of a well-defined and much simpler chemical structure, potentially facilitating the interpretation of its role in adsorption mechanisms.

In this work, the citrate concentration was increased from the original concentration of 1 mM in the as-synthesized AuNP suspension to an upper limit of 7.5 mM. It can be seen from Fig. 3a that the adsorption of AuNPs generally increased with increasing citrate concentration. At a citrate concentration of 7.5 mM, nearly full adsorption of AuNPs on illite could be achieved, which is significantly greater than the 70% AuNP adsorption at a citrate concentration of 1 mM. In addition, the time needed to reach the equilibrium c/c_0 value decreased with increasing citrate concentration, indicating an increased AuNP adsorption rate after citrate addition.

In general, the stability of NPs in a suspension increases with increasing ligand concentration due to enhanced surface complexation. As shown in Fig. 3b, the ζ-potential of our negatively charged AuNPs did become more negative with increasing citrate concentration, suggesting greater citrate coverage on the surface of the AuNPs (Wagener *et al.*, 2012). Similarly, the measured adsorption of citrate on illite (Fig. 3c) and thus the absolute value of the illite ζ-potential (Fig. 3d) also increased after citrate adsorption. Such more negative ζ-potential values of both AuNPs and illite should result in greater electric repulsion between particles and contribute to less adsorption of AuNPs. Additionally, the competitive adsorption of citrate on illite edges could also lead to reduced AuNP adsorption. The above

mechanisms, although supported by many previous studies (Yang *et al.*, 2013; Wang *et al.*, 2015b; Dong & Zhou, 2020; Guo *et al.*, 2020), do not agree with the observed increased AuNP adsorption at greater citrate concentrations in our work, suggesting that some other role of citrate must be contributing to the improved AuNP adsorption. The well-known destabilizing bridging role is considered minor for citrate in our experiments, as bridging between particles normally occurs with larger organic molecules at relatively low concentrations (Philippe & Schaumann, 2014; Yu *et al.*, 2018; Ahmed *et al.*, 2021). Under high solid/liquid ratio and initial pH conditions, the pH buffering effect of citrate (a tricarboxylic acid anion) deserves attention because pH is a decisive factor in adsorption, and the presence of a large amount of illite is known to cause considerable change in the pH of a system (see Fig. S5). As shown in Fig. S6, the addition of citrate reduced the increase in pH from the initial value (pH 4) to the final value. For example, the final pH became ∼4.2 when the citrate concentration was 7.5 mM, compared with the final pH of 4.9 at the original citrate concentration of 1.0 mM. Although this buffering effect may seem to have caused only a small difference in the final pH, the resulting lower pH (at greater citrate concentrations) should be sufficiently favourable to create more positively charged sites at the illite edge (see Fig. S4b), enabling the adsorption of more AuNPs (compared with the effect of an initial pH of 4.0–4.5 presented above). Additionally, an increase in citrate anion concentration increases the IS of the system, which, as shown above, can screen the electrostatic repulsion between negatively charged particles and thus promote their (hetero)aggregation (Johnson & Lenhoff, 1996; Sadowska *et al.*, 2014). Finally, the addition of citrate can facilitate the dissolution of illite (Table S2), which not only significantly increases the IS of the suspension, but also releases some high-valence framework ions, having a strong effect on aggregation according to the empirical Schulze–Hardy rule (Yecheskel *et al.*, 2019; Dong & Zhou, 2020) and therefore promoting AuNP adsorption substantially.
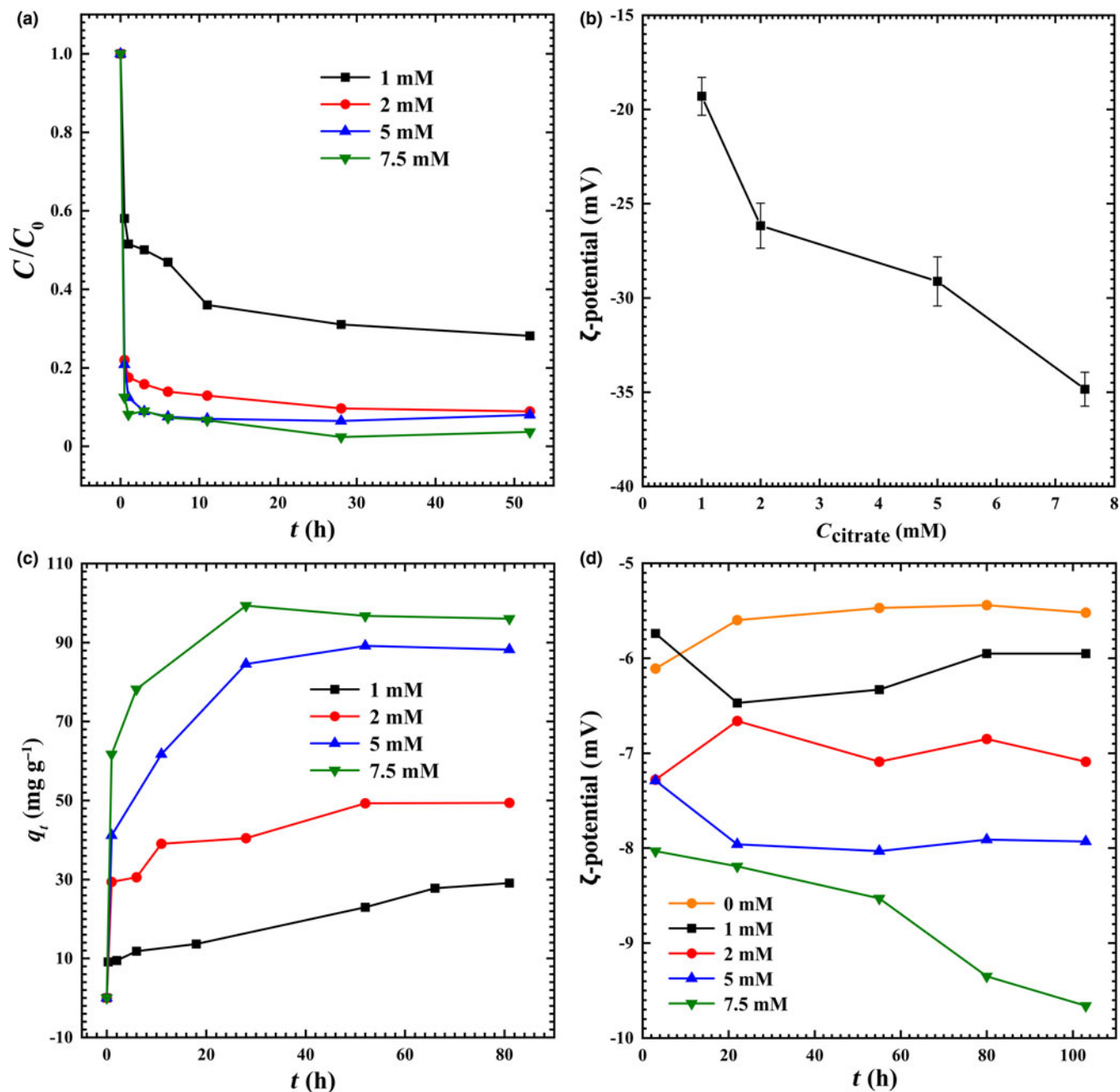
Figure 3. (a) Effect of citrate concentration (1.0–7.5 mM) on the adsorption of AuNPs. (b) ζ-potential of AuNPs at various citrate concentrations. (c) The adsorption of citrate on illite at various citrate concentrations (without AuNPs). (d) ζ-potential of illite at various citrate concentrations (without AuNPs).

Effect of temperature on the adsorption process

Temperature can affect the thermodynamics and kinetics of adsorption processes profoundly (Freitas & Muller, 1998; Das, 2017). Figure 4a shows the overall effect of temperature on the adsorption of AuNPs on illite. Specifically, a significant increase in the adsorption rate during the initial hours of the experiment was found at greater temperatures, which is attributed to the known more rapid kinetics promoted by increased temperature. In addition, when the temperature of the system increased from 5 to 60°C, the equilibrium adsorbed amount of AuNPs on illite increased from ~70% to 95%. Such increased AuNP adsorption on illite with increasing temperature is explained by the following

aspects: primarily, it is important to note that the absolute ζ-potential values of AuNPs (Fig. 4b) and illite (Fig. 4c) both decreased with increasing temperature. For example, when the temperature was increased from 5 to 60°C, the ζ-potential values of AuNPs and illite changed from –35 to –12 mV and from –12 to –1 mV, respectively. The reduced absolute ζ-potential value of AuNPs with increasing temperature was ascribed partly to the increased pK_a value of citric acid, which corresponds to the reduced extent of citric acid dissociation and therefore number of negative charges on the surface of AuNPs (Goldberg *et al.*, 2002). In addition, as demonstrated in Table S3, increasing temperature also promoted the dissolution of illite (involving the release of high-valence framework cations), which increased the IS of the
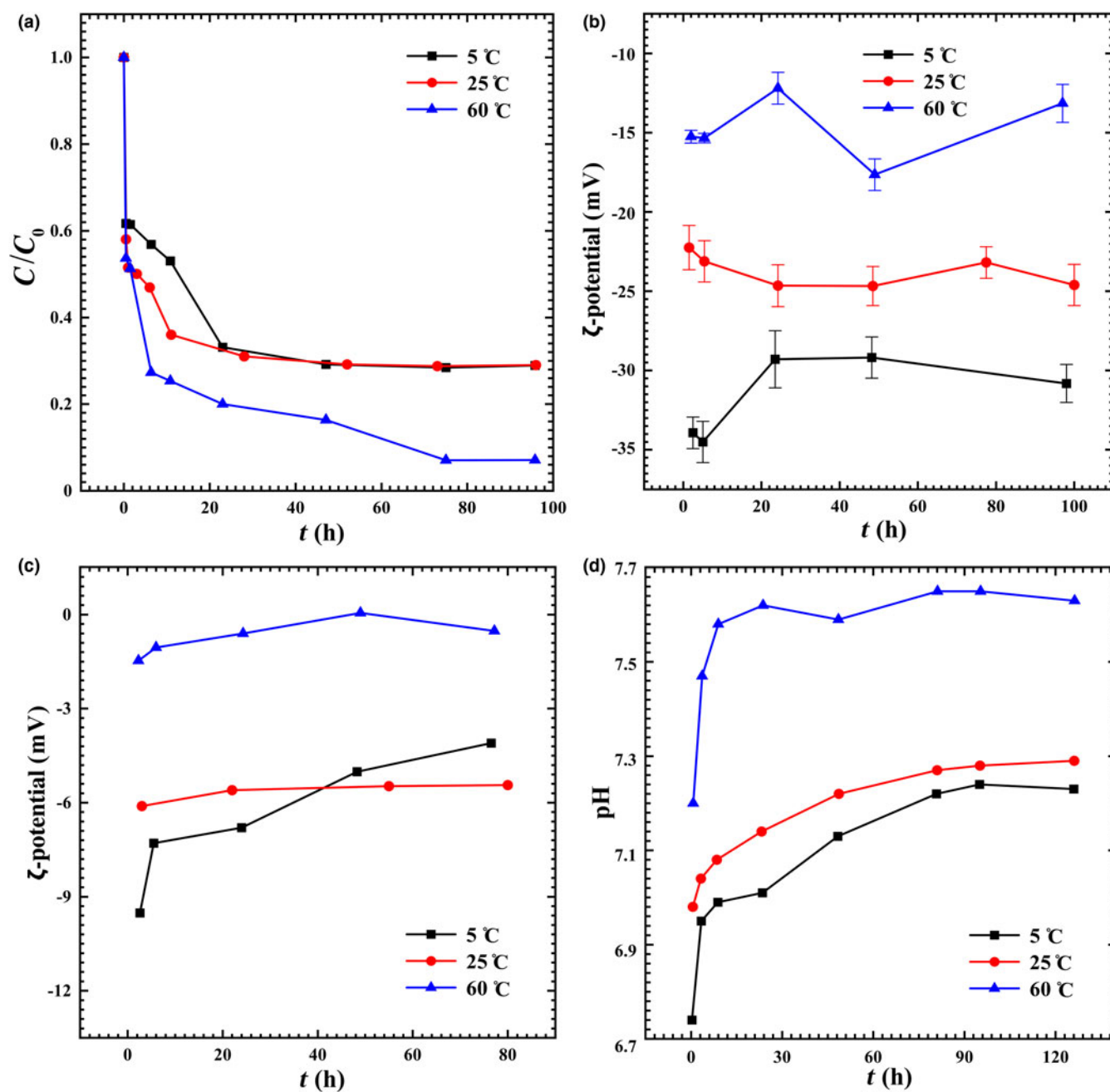
Figure 4. (a) Effect of temperature on the adsorption of AuNPs on illite. (b) ζ-potential of AuNPs at various temperatures. (c) ζ-potential of illite at various temperatures. (d) pH changes of illite in deionized water at various temperatures.
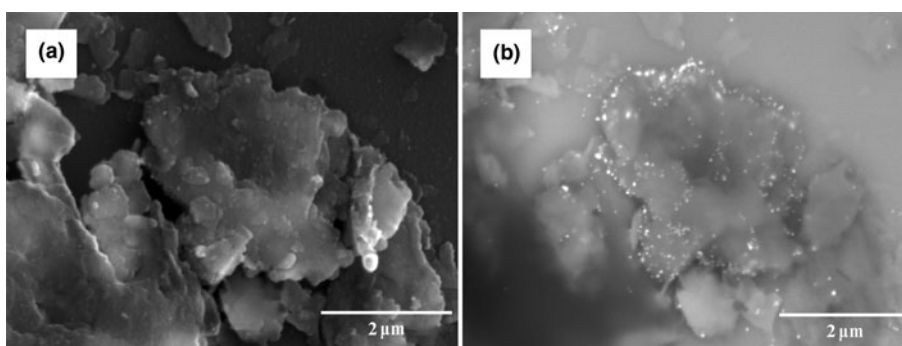
Figure 5. SEM images of illite after adsorption of AuNPs at 60℃: (a) secondary electron images, (b) backscattered electron images.
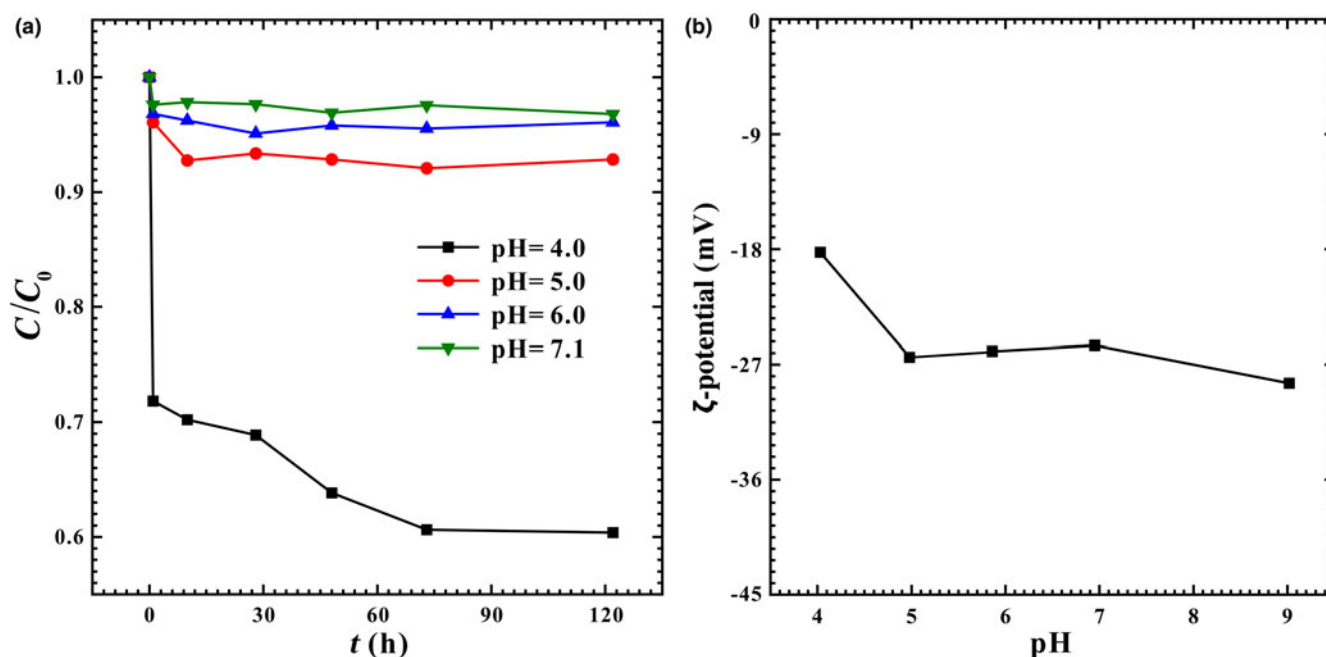
Figure 6. (a) Effect of pH on the adsorption of AuNPs on illite (∼74 μm). (b) ζ-potential of illite (∼74 μm).

suspension and in turn contributed to decreasing the absolute ζ-potential values of both AuNPs and illite. The lowering of absolute ζ-potential values, which reduces the electrostatic repulsion, along with the release of high-valence cations that promote aggregations, made it easier for AuNPs to adsorb on the edges of illite. As shown in Fig. 5, numerous AuNPs were adsorbed on the edge face of illite at 60°C, which is consistent with our previous observations (Fu *et al.*, 2020).

Effect of illite particle size on the adsorption process

Natural mineral particles exist in a range of particle sizes, and these varying sizes could play a role in the AuNP adsorption process. To explore the effect of illite particle size, illite with a greater particle size of ∼74 μm was selected for use in adsorption experiments at pH 4–7. Compared with the aforementioned experiments with illite of smaller size (<2 μm), a similar trend in the variation of pH was displayed for the experiments with larger-sized illite particles (see Fig. 6a). That is, the adsorption of AuNPs always decreased with increasing pH. The difference is that the larger-sized illite particles appeared to adsorb fewer AuNPs than the smaller-sized illite particles under the same experimental conditions. At pH 4, compared with 70% AuNP adsorption on the smaller-sized illite, only 40% of AuNPs were adsorbed on the larger-sized illite, whereas at pH 6 (and higher) only <5% of AuNPs were adsorbed on the larger-sized illite (Fig. 6a). The ζ-potential measurements indicated that the larger-sized illite displays approximately two times more negative ζ-potential values than the smaller-sized illite across the whole pH 4–9 range (compare Fig. 6b with Fig. S4a). The reasons for the significant difference in AuNP adsorption between illite particles of various sizes may be twofold: first, the smaller-sized illite exposes more edge sites capable of adsorbing AuNPs; and second, because of there being relatively more positive charges on the exposed edge faces of the smaller-sized illite, the overall ζ-potential becomes less negative and thus exerts less electrostatic repulsion on the approaching AuNPs.

Desorption of negatively charged AuNPs

Whether and to what extent NPs can desorb from mineral surfaces is important, in that desorption behaviour influences the fate and transport of NPs directly and also provides some useful insights into the adsorption mechanism. Thus, we carried out desorption experiments by first obtaining illite from the adsorption suspension (initial pH 4) through centrifugation, and then, with a constant solid/liquid ratio maintained at 5 g L^{-1}, adding deionized water (pH 4) with or without 1 mM citrate to the
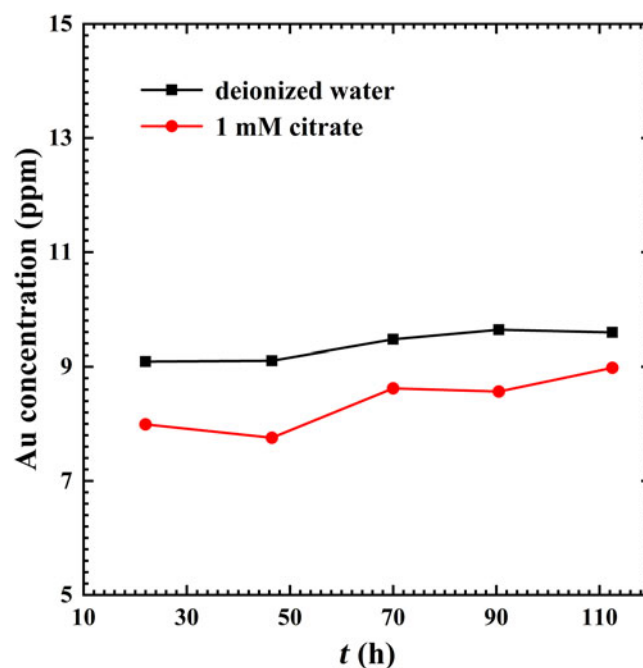

Figure 7. Au concentration in the supernatant after the desorption experiment.

separated illite. The results of the desorption experiments are shown in Fig. 7. Up to ~9 ppm (slightly more than 20%) of the pre-adsorbed AuNPs were desorbed from illite after exposure to deionized water or sodium citrate solution, implying that the majority of the adsorbed AuNPs might be bonded firmly to the edge sites of illite. In other words, from an energy perspective, we believe that most AuNPs were deposited in the primary energy minima (instead of the secondary energy minima) according to DLVO theory, and the reversible release of such adsorbed AuNPs following changes in solution chemistry is considered improbable. Additionally, Fig. 7 also shows that the amount of AuNPs desorbed in water was greater than that in 1 mM citrate, which demonstrates inhibition of AuNP desorption due to the presence of citrate and is consistent with the result of citrate promoting AuNP adsorption as discussed above.

Conclusion

We conducted a systematic study of the adsorption behaviour of negatively charged AuNPs on illite under conditions of relatively high solid/liquid ratios and initial pH. The adsorbed amount of AuNPs, which can vary widely from being negligible (much less than 5%) to nearly complete (up to 100%), was found to decrease with increasing pH or illite particle size and to increase with increasing IS, citrate concentration and temperature. Upon investigation of the effects of the above key factors, a number of complex processes and mechanisms have been identified that control AuNP adsorption behaviour, and the structural and charge heterogeneity of illite have been demonstrated also to play a substantial role. Under our experimental conditions, the suspension pH can be changed significantly with the presence of illite through interlayer cation exchange, edge face hydroxyl protonation and dissolution. The suspension pH and other solution chemistry parameters (IS, citrate concentration, etc.) modulate the electrostatic interaction between illite and AuNPs, which is considered to be the dominant mechanism in the AuNP adsorption process (as summarized in Fig. 8). At pH values greater than the pH_{PZC}, both the basal plane and edge face of illite are negatively charged, and the electrical repulsion between illite and negatively charged AuNPs is strong enough to prevent any significant adsorption. However, at pH values lower than the pH_{PZC}, the illite edge becomes positively charged, resulting in electrostatic attraction and considerable adsorption of AuNPs at the edge sites. The addition of salt to the suspension either directly or through the dissolution of illite (promoted by increased temperature or citrate concentration) can suppress the EDL repulsion between particles
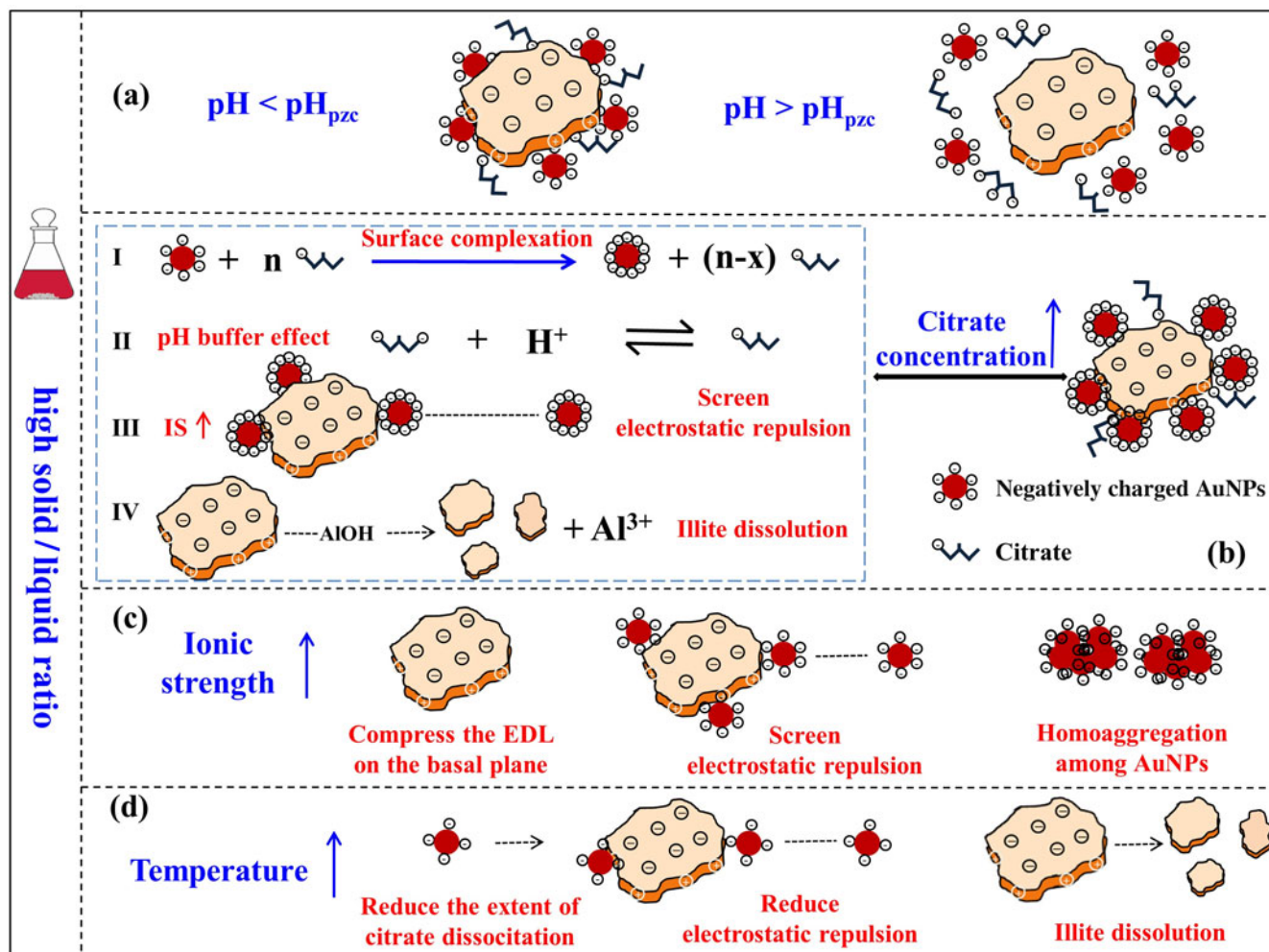
Figure 8. Schematic representation of the mechanism of adsorption of negatively charged AuNPs under various conditions: (a) pH, (b) citrate concentration, (c) IS, (d) temperature.

and thus facilitate the adsorption and aggregation processes. The pH buffering role of citrate is also proposed to contribute to the increased AuNP adsorption at greater citrate concentrations. Finally, our desorption experiments suggest that most adsorbed AuNPs are bonded strongly with illite, possibly in the primary energy trap. The results from this work are expected to provide new and valuable information applicable to many natural and engineering processes that involve migration and enrichment of elements in NPs. Based on the findings of this work, future studies could aim to further predict or optimize NP adsorption processes to expand the application of clay minerals and NPs in environmental management, catalysis, photoreactions, biomedicine and other fields.

Conflicts of interest. The authors declare none.

Supplementary material. To view supplementary material for this article, please visit https://doi.org/10.1180/clm.2023.23.

References

Abbas Q., Yousaf B., Amina, A.M.U., Munir M.A.M., El-Naggar A., Rinklebe J. & Naushad M. (2020a) Transformation pathways and fate of engineered nanoparticles (ENPs) in distinct interactive environmental compartments: a review. *Environment International*, **138**, 105646.

Abbas Q., Yousaf B., Ullah H., Ali M.U., Ok Y.S. & Rinklebe J. (2020b) Environmental transformation and nano-toxicity of engineered nanoparticles (ENPs) in aquatic and terrestrial organisms. *Critical Reviews in Environmental Science and Technology*, **50**, 2523–2581.

Ahmed B., Rizvi A., Ali K., Lee J., Zaidi A., Khan M.S. & Musarrat J. (2021) Nanoparticles in the soil–plant system: a review. *Environmental Chemistry Letters*, **19**, 1545–1609.

Alvarez-Puebla R.A., Arceo E., Goulet P.J.G., Garrido J.J. & Aroca R.F. (2005) Role of nanoparticle surface charge in surface-enhanced Raman scattering. *Journal of Physical Chemistry B*, **109**, 3787–3792.

Amde M., Liu J.F., Tan Z.Q. & Bekana D. (2017) Transformation and bioavailability of metal oxide nanoparticles in aquatic and terrestrial environments. A review. *Environmental Pollution*, **230**, 250–267.

Avena M. (2003) Proton binding at clay surfaces in water. *Applied Clay Science*, **24**, 3–9.

Bakken B.M., Hochella M.F., Marshall A.F. & Turner A.M. (1989) High-resolution microscopy of gold in unoxidized ore from the Carlin mine, Nevada. *Economic Geology*, **84**, 171–179.

Barton L.E., Therezien M., Auffan M., Bottero J.Y. & Wiesner M.R. (2014) Theory and methodology for determining nanoparticle affinity for heteroaggregation in environmental matrices using batch measurements. *Environmental Engineering Science*, **31**, 421–427.

Bedelean H., Maicaneanu A., Burca S. & Stanca M. (2009) Removal of heavy metal ions from wastewaters using natural clays. *Clay Minerals*, **44**, 487–495.

Bergaya F. & Lagaly G., editors (2013) *Handbook of Clay Science*. Elsevier, Amsterdam, The Netherlands, 84 pp.

Bond G.C. & Thompson D.T. (2006) Status of catalysis by gold following an AURICAT Workshop. *Applied Catalysis A – General*, **302**, 1–4.

Borm P.J.A., Robbins D., Haubold S., Kuhlbusch T., Fissan H., Donaldson K. *et al.* (2006) The potential risks of nanomaterials: a review carried out for ECETOC. *Particle and Fibre Toxicology*, **3**, 11.

Braissant O., Verrecchia E.P. & Aragno M. (2002) Is the contribution of bacteria to terrestrial carbon budget greatly underestimated? *Science of Nature*, **89**, 366–370.

Brar S.K., Verma M., Tyagi R.D. & Surampalli R.Y. (2010) Engineered nanoparticles in wastewater and wastewater sludge – evidence and impacts. *Waste Management*, **30**, 504–520.

Buzea C., Pacheco I.I. & Robbie K. (2007) Nanomaterials and nanoparticles: sources and toxicity. *Biointerphases*, **2**, MR17–MR71.

Cao J.J. & Cheng S.T. (2020) Characteristics of particles in groundwater and their prospecting significance for the Shijiangshan Pb–Zn–Ag deposit, Inner Mongolia, China. *Journal of Geochemical Exploration*, **217**, 106592.

Chen H., Chen Y.G., Zheng X., Li X. & Luo, J.Y. (2014) How does the entering of copper nanoparticles into biological wastewater treatment system affect sludge treatment for VFA production. *Water Research*, **63**, 125–134.

Cottet L., Almeida C.A.P., Naidek N., Viante M.F., Lopes M.C. & Debacher N.A. (2014) Adsorption characteristics of montmorillonite clay modified with iron oxide with respect to methylene blue in aqueous media. *Applied Clay Science*, **95**, 25–31.

Das P.K. (2017) Effect of temperature on zeta potential of functionalized gold nanorod. *Microfluidics and Nanofluidics*, **21**, 95.

de Barros A., Constantino C.J.L., da Cruz N.C., Bortoleto, J.R.R. & Ferreira M. (2017) High performance of electrochemical sensors based on LbL films of gold nanoparticles, polyaniline and sodium montmorillonite clay mineral for simultaneous detection of metal ions. *Electrochimica Acta*, **235**, 700–708.

Delhorme M., Labbez C., Caillet C. & Thomas F. (2010) Acid–base properties of 2:1 clays. I. Modeling the role of electrostatics. *Langmuir*, **26**, 9240–9249.

Derjaguin B.V. & Landau L. (1941) Theory of the stability of strongly charged lyophobic sols and of the adhesion of strongly charged particles in solutions of electrolytes. *Acta Physicochimica USSR*, **14**, 633–662.

Dong F. & Zhou Y. (2020) Distinct mechanisms in the heteroaggregation of silver nanoparticles with mineral and microbial colloids. *Water Research*, **170**, 115332.

Elimelech M., Gregory J., Jia X. & Williams R.A., editors (1995) *Particle Deposition and Aggregation: Measurement, Modelling and Simulation*. Butterworth-Heinemann, Oxford, UK, 261–423 pp.

Floody M.C., Theng B.K.G., Reyes P. & Mora M.L. (2009) Natural nanoclays: applications and future trends – a Chilean perspective. *Clay Minerals*, **44**, 161–176.

Freitas C. & Muller R.H. (1998) Effect of light and temperature on zeta potential and physical stability in solid lipid nanoparticle (SLN™) dispersions. *International Journal of Pharmaceutics*, **168**, 221–229.

Frens G. (1973) Controlled nucleation for regulation of particle-size in monodisperse gold suspensions. *Nature – Physical Science*, **241**, 20–22.

Frondel C. (1938) Stability of colloidal gold under hydrothermal conditions. *Economic Geology*, **33**, 1–20.

Fu Y.H., Nie X., Qin Z.H., Li S.S. & Wan Q. (2017) Effect of particle size and pyrite oxidation on the sorption of gold nanoparticles on the surface of pyrit. *Journal of Nanoscience and Nanotechnology*, **17**, 6367–6376.

Fu Y.H., Qin Z.H., Nie X., Li S.S. & Wan Q. (2020) The effect of pH on the sorption of gold nanoparticles on illite. *Acta Geochimica*, **39**, 172–180.

Gaines G.L. & Vedder W. (1964) Dehydroxylation of muscovite. *Nature*, **201**, 495.

Gallego-Urrea J.A., Hammes J., Cornelis G. & Hassellöv M. (2016) Coagulation and sedimentation of gold nanoparticles and illite in model natural waters: influence of initial particle concentration. *NanoImpact*, **3–4**, 67–74.

Goldberg R.N., Kishore N. & Lennen R.M. (2002) Thermodynamic quantities for the ionization reactions of buffers. *Journal of Physical and Chemical Reference Data*, **31**, 231–370.

Gradusov B.P. (1974) A tentative study of clay mineral distribution in soils of the world. *Geoderma*, **12**, 49–55.

Guo Q.Y., Wang Z.Q., Xu Q.J, Mao H., Zhang D., Ghosh S. *et al.* (2020) Suspended state heteroaggregation kinetics of kaolinite and fullerene (nC_{60}) in the presence of tannic acid: effect of π–π interactions. *Science of the Total Environmental*, **713**, 136559.

Hannington M., Haroardottir V., Garbe-Schoenberg D. & Brown K.L. (2016) Gold enrichment in active geothermal systems by accumulating colloidal suspensions. *Nature Geoscience*, **9**, 299–303.

Hendren C.O., Mesnard X., Droge J. & Wiesner M.R. (2011) Estimating production data for five engineered nanomaterials as a basis for exposure assessment. *Environmental Science & Technology*, **45**, 2562–2569.

Hochella M.F. (2002) Nanoscience and technology the next revolution in the Earth sciences. *Earth and Planetary Science Letters*, **203**, 593–605.

Hochella M.F., Lower S.K., Maurice P.A., Penn R.L., Sahai N., Sparks D.L. & Twining B.S. (2008) Nanominerals, mineral nanoparticles, and Earth systems. *Science*, **319**, 1631–1635.

Hochella M.F., Mogk D.W., Ranville J., Allen I.C., Luther G.W., Marr L.C. *et al.* (2019) Natural, incidental, and engineered nanomaterials and their impacts on the Earth system. *Science*, **363**, 1414–1423.

Hong H.L., Wang Q.Y., Chang J.P., Liu S.R. & Hu R.Z. (1999) Occurrence and distribution of invisible gold in the Shewushan supergene gold deposit, southeastern Hubei, China. *Canadian Mineralogist*, **37**, 1525–1531.

Hotze E.M., Phenrat T. & Lowry G.V. (2010) Nanoparticle aggregation: challenges to understanding transport and reactivity in the environment. *Journal of Environmental Quality*, **39**, 1909–1924.

Hough R.M., Noble R.R.P. & Reich M. (2011) Natural gold nanoparticles. *Ore Geology Reviews*, **42**, 55–61.

Hough R.M., Noble R.R.F., Hitchen G.J., Hart R., Reddy S.M., Saunders M. *et al.* (2008) Naturally occurring gold nanoparticles and nanoplates. *Geology*, **36**, 571–574.

Hu G., Cao J.J., Wang C.Y., Lu M.Q. & Lin Z.X. (2020) Study on the characteristics of naturally formed TiO$_2$ nanoparticles in various surficial media from China. *Chemical Geology*, **550**, 119703.

Huang G.X., Guo H.Y., Zhao J, Liu Y.H. & Xing B.S. (2016) Effect of co-existing kaolinite and goethite on the aggregation of graphene oxide in the aquatic environment. *Water Research*, **102**, 313–320.

Huertas F.J., Chou L. & Wollast R. (2001) Kaolinite dissolution rates in batch experiments at room temperature and pressure: reply to 'On the interpretation of closed system mineral dissolution experiments,' comment by Eric H. Oelkers, Jacques Schott, and Jean-Luc Devidal. *Geochimica et Cosmochimica Acta*, **65**, 4433–4434.

Johnson C.A. & Lenhoff A.M. (1996) Adsorption of charged latex particles on mica studied by atomic force microscopy. *Journal of Colloid and Interface Science*, **179**, 587–599.

Keller A.A., McFerran S., Lazareva A. & Suh S. (2013) Global life cycle releases of engineered nanomaterials. *Journal of Nanoparticle Research*, **15**, 1692.

King J., Williams-Jones A.E., van Hinsberg V. & Williams-Jones G. (2014) High-sulfidation epithermal pyrite-hosted Au (Ag–Cu) ore formation by condensed magmatic vapors on Sangihe Island, Indonesia. *Economic Geology*, **109**, 1705–1733.

Kusebauch C., Oelze M. & Gleeson S.A. (2018) Partitioning of arsenic between hydrothermal fluid and pyrite during experimental siderite replacement. *Chemical Geology*, **500**, 136–147.

Kusebauch C., Gleeson S.A. & Oelze M. (2019) Coupled partitioning of Au and As into pyrite controls formation of giant Au deposits. *Science Advances*, **5**, eaav5891.

Labille J., Harns C., Bottero J.Y. & Brant J. (2015) Heteroaggregation of titanium dioxide nanoparticles with natural clay colloids. *Environmental Science & Technology*, **49**, 6608–6616.

Lintern M., Anand R., Ryan C. & Paterson D. (2013) Natural gold particles in Eucalyptus leaves and their relevance to exploration for buried gold deposits. *Nature Communications*, **4**, 2614.

Liu X.D., Lu X.C., Sprik M., Cheng J., Meijer E.J. & Wang R.C. (2013) Acidity of edge surface sites of montmorillonite and kaolinite. *Geochimica et Cosmochimica Acta*, **117**, 180–190.

Liu X.D., Cheng J., Sprik M., Lu X.C. & Wang R.C. (2014) Surface acidity of 2:1-type dioctahedral clay minerals from first principles molecular dynamics simulations. *Geochimica et Cosmochimica Acta*, **140**, 410–417.

Liu J.B., Hwang Y.S. & Lenhart J.J. (2015) Heteroaggregation of bare silver nanoparticles with clay minerals. *Environmental Science – Nano*, **2**, 528–540.

Li X., He E., Zhang M.Y., Peijnenburg W.J.G.M., Liu Y., Song L. *et al.* (2020) Interactions of CeO$_2$ nanoparticles with natural colloids and electrolytes impact their aggregation kinetics and colloidal stability. *Journal of Hazardous Materials*, **386**, 121973.

Luo S.X., Nie X., Yang M.Z., Fu Y.H., Zeng P. & Wan Q. (2018) Sorption of differently charged gold nanoparticles on synthetic pyrite. *Minerals*, **8**, 428.

Lu X.Y., Lu T.T., Zhang H.J., Shang Z.B., Chen J.Y., Wang Y. *et al.* (2019) Effects of solution chemistry on the attachment of graphene oxide onto clay minerals. *Environmental Science – Process & Impacts*, **21**, 506–513.

Machado S., Stawinski W., Slonina P., Pinto A.R., Grosso J.P., Nouws H.P. *et al.* (2013) Application of green zero-valent iron nanoparticles to the remediation of soils contaminated with ibuprofen. *Science of the Total Environment*, **461**, 323–329.

Mackenzie R.C. & Mitchell B.D. (1966) Clay mineralogy. *Earth Science Reviews*, **2**, 47–91.

Martin S.A., Valdes L., Merida F., de Menorval L.C., Velazquez M. & Rivera A. (2018) Natural clay from Cuba for environmental remediation. *Clay Minerals*, **53**, 193–201.

McLeish D.F., Williams-Jones A.E., Vasyukova O.V., Clark J.R. & Board W.S. (2021) Colloidal transport and flocculation are the cause of the hyperenrichment of gold in nature. *Proceedings of the National Academy of Sciences of the United States of Amecica*, **118**, e2100689118.

Mikhlin Y.L. & Romanchenko A.S. (2007) Gold deposition on pyrite and the common sulfide minerals: an STM/STS and SR-XPS study of surface reactions and Au nanoparticles. *Geochimica et Cosmochimica Acta*, **71**, 5985–6001.

Novikov A.P., Kalmykov S.N., Utsunomiya S., Ewing R.C., Horreard F., Merkulov A. *et al.* (2006) Colloid transport of plutonium in the far-field of the Mayak Production Association, Russia. *Science*, **314**, 638–641.

Nowack B. & Bucheli T.D. (2007) Occurrence, behavior and effects of nanoparticles in the environment. *Environmental Pollution*, **150**, 5–22.

Palenik C.S., Utsunomiya S., Reich M., Kesler S.E., Wang L.M. & Ewing R.C. (2004) 'Invisible' gold revealed: direct imaging of gold nanoparticles in a Carlin-type deposit. *American Mineralogist*, **89**, 1359–1366.

Petosa A.R., Jaisi D.P., Quevedo I.R., Elimelech M. & Tufenkji N. (2010) Aggregation and deposition of engineered nanomaterials in aquatic environments: role of physicochemical interactions. *Environmental Science & Technology*, **44**, 6532–6549.

Petrella L., Thébaud N., Fougerouse D., Evans K., Quadir Z. & Laflamme C. (2020) Colloidal gold transport: a key to high-grade gold mineralization? *Mineralium Deposita*, **55**, 1247–1254.

Petrella L., Thébaud N., Fougerouse D., Tattitch B., Martin L., Turner S. *et al.* (2022) Nanoparticle suspensions from carbon-rich fluid make high-grade gold deposits. *Nature Communications*, **13**, 3795.

Philippe A. & Schaumann G.E. (2014) Interactions of dissolved organic matter with natural and engineered inorganic colloids: a review. *Environmental Science & Technology*, **48**, 8946–8962.

Praetorius A., Badetti E., Brunelli A., Clavier A., Gallego-Urrea J.A., Gondikas A. *et al.* (2020) Strategies for determining heteroaggregation attachment efficiencies of engineered nanoparticles in aquatic environments. *Environmental Science – Nano*, **7**, 351–367.

Ramos M.E. & Huertas F.J. (2014) Adsorption of lactate and citrate on montmorillonite in aqueous solutions. *Applied Clay Science*, **90**, 27–34.

Rawat S., Pullagurala V.L.R., Adisa I.O., Wang Y., Peralta-Videa J.R. & Gardea-Torresdey J.L. (2018) Factors affecting fate and transport of engineered nanomaterials in terrestrial environments. *Current Opinion in Environmental Science & Health*, **6**, 47–53.

Reich M., Kesler S.E., Utsunomiya S., Palenik C.S., Chryssoulis S.L. & Ewing R.C. (2005) Solubility of gold in arsenian pyrite. *Geochimica et Cosmochimica Acta*, **69**, 2781–2796.

Reith F. & Cornelis G. (2017) Effect of soil properties on gold- and platinum nanoparticle mobility. *Chemical Geology*, **466**, 446–453.

Ryan P.R., Delhaize E. & Jones D.L. (2001) Function and mechanism of organic anion exudation from plant roots. *Annual Review of Plant Biology*, **52**, 527–560.

Sadowska M., Adamczyk Z. & Nattich-Rak M. (2014) Mechanism of nanoparticle deposition on polystyrene latex particles. *Langmuir*, **30**, 692–699.

Saka E.E. & Gueler C. (2006) The effects of electrolyte concentration, ion species and pH on the zeta potential and electrokinetic charge density of montmorillonite. *Clay Minerals*, **41**, 853–861.

Sathuluri R.R., Yoshikawa H., Shimizu E., Saito M. & Tamiya E. (2011) Gold nanoparticle-based surface-enhanced Raman scattering for noninvasive molecular probing of embryonic stem cell differentiation. *PLoS ONE*, **6**, e22802.

Saunders J.A. & Burke M. (2017) Formation and aggregation of gold (electrum) nanoparticles in epithermal ores. *Minerals*, **7**, 163.

Saunders J.A., Burke M. & Brueseke M.E. (2020) Scanning-electron-microscope imaging of gold (electrum) nanoparticles in middle Miocene bonanza epithermal ores from northern Nevada, USA. *Mineralium Deposita*, **55**, 389–398.

Schomburg J. & Zwahr H. (1997) Thermal differential diagnosis of mica mineral group. *Journal of Thermal Analysis and Calorimetry*, **48**, 135–139.

Sharma V.K., Filip J., Zboril R. & Varma R.S. (2015) Natural inorganic nanoparticles – formation, fate, and toxicity in the environment. *Chemical Society Reviews*, **44**, 8410–8423.

Sharma V.K., Sayes C.M., Guo B.L., Pillai S., Parsons J.G., Wang C.Y. *et al.* (2019) Interactions between silver nanoparticles and other metal nanoparticles under environmentally relevant conditions: a review. *Science of the Total Environment*, **653**, 1042–1051.

Slomberg D.L., Ollivier P., Radakovitch O., Baran N., Sani-Kast N., Bruchet A. *et al.* (2017) Insights into natural organic matter and pesticide characterisation and distribution in the Rhone River. *Environmental Chemistry*, **14**, 64–73.

Sotirelis N.P. & Chrysikopoulos C.V. (2016) Heteroaggregation of graphene oxide nanoparticles and kaolinite colloids. *Science of the Total Environment*, **579**, 736–744.

Southam G., Lengke M.F., Fairbrother L. & Reith F. (2009) The biogeochemistry of gold. *Elements*, **5**, 303–307.

Spurgeon D.J., Lahive E. & Schultz C.L. (2020) Nanomaterial transformations in the environment: effects of changing exposure forms on bioaccumulation and toxicity. *Small*, **16**, 2000618.

Syngouna V.I., Giannadakis G.I. & Chrysikopoulos C.V. (2018) Interaction of graphene oxide nanoparticles with quartz sand and montmorillonite colloids. *Environmental Technology*, **41**, 1127–1138.

Tang Z. & Cheng T. (2018) Stability and aggregation of nanoscale titanium dioxide particle (nTiO$_2$): effect of cation valence, humic acid, and clay colloids. *Chemosphere*, **192**, 51–58.

Thill A., Moustier S., Garnier J.M., Estournel C., Naudin J.J. & Bottero J.Y. (2001) Evolution of particle size and concentration in the Rhone River mixing zone: influence of salt flocculation. *Continental Shelf Reasearch*, **21**, 2127–2140.

Thio B.J.R., Lee J.H., Meredith J.C. & Keller, A.A. (2010) Measuring the influence of solution chemistry on the adhesion of Au nanoparticles to mica using colloid probe atomic force microscopy. *Langmuir*, **26**, 13995–14003.

Tiede K., Hassellov M., Breitbarth E., Chaudhry Q. & Boxall A.B.A. (2009) Considerations for environmental fate and ecotoxity testing to support environmental risk assessments for engineered nanoparticles. *Journal of Chromatography A*, **1216**, 503–509.

Tombácz E. & Szekeres M. (2004) Colloidal behavior of aqueous montmorillonite suspensions: the specific role of pH in the presence of indifferent electrolytes. *Applied Clay Science*, **27**, 75–94.

Verwey F.J.W. & Overbeek J.T.G., editors (1948) *Theory of the Stability of Lyophobic Colloids*. Elsevier, Amsterdam, The Netherlands, 205 pp.

Wagener P., Schwenke A. & Barcikowski S. (2012) How citrate ligands affect nanoparticle adsorption to microparticle supports. *Langmuir*, **28**, 6132–6140.

Wang H.T., Adeleye A.S., Huang Y.X., Li F.T. & Keller A.A. (2015a) Heteroaggregation of nanoparticles with biocolloids and geocolloids. *Advances in Colloid and Interface Science*, **226**, 24–36.

Wang H.T., Dong Y.N., Zhu M., Li X., Keller A.A., Wang T. & Li F.T. (2015b) Heteroaggregation of engineered nanoparticles and kaolin clays in aqueous environments. *Water Research*, **80**, 130–138.

Wang Z.Y., Cao J.J., Lin Z.X. & Wu Z.Q. (2016) Characteristics of soil particles in the Xiaohulishan deposit, Inner Mongolia, China. *Journal of Geochemical Exploration*, **169**, 30–42.

Wang Y.L., Yang K., Chefetz B., Xing B.S. & Lin D.H. (2019) The pH and concentration dependent interfacial interaction and heteroaggregation between nanoparticulate zero-valent iron and clay mineral particles. *Environmental Science – Nano*, **6**, 2129–2140.

Wang X., Peng K.Q., Hu Y., Zhang F.Q., Hu B., Li L. *et al.* (2014) Silicon/hematite core/shell nanowire array decorated with gold nanoparticles for unbiased solar water oxidation. *Nano Letters*, **14**, 18–23.

Wang J.Y., Zhao X.L., Wu F.C., Tang Z., Zhao T.H., Niu L. *et al.* (2021) Impact of montmorillonite clay on the homo- and heteroaggregation of titanium dioxide nanoparticles (nTiO$_2$) in synthetic and natural waters. *Science of the Total Environment*, **784**, 147019.

Ward D.B. & Brady P.V. (1998) Effect of Al and organic acids on the surface chemistry of kaolinite. *Clays and Clay Minerals*, **46**, 453–465.

Wierchowiec J., Mikulski S.Z. & Zieliński K. (2021) Supergene gold mineralization from exploited placer deposits at Dziwiszów in the Sudetes (NE Bohemian Massif, SW Poland). *Ore Geology Reviews*, **131**, 104049.

Yang Z., Yan H., Yang H., Li H., Li A. & Cheng R. (2013) Flocculation performance and mechanism of graphene oxide for removal of various contaminants from water. *Water Research*, **47**, 3037–3046.

Yecheskel Y., Dror I. & Berkowitz B. (2019) Effect of phosphate, sulfate, arsenate, and pyrite on surface transformations and chemical retention of gold nanoparticles (Au-NPs) in partially saturated soil columns. *Environmental Science & Technology*, **53**, 13071–13080.

Yu S.J., Liu J.F., Yin Y.G. & Shen M.H. (2018) Interactions between engineered nanoparticles and dissolved organic matter: a review on mechanisms and environmental effects. *Journal of Environmental Sciences*, **63**, 198–217.

Yu W.B., Xu H.F., Roden E.E. & Wan Q. (2019) Efficient adsorption of iodide from water by chrysotile bundles with wedge-shaped nanopores. *Applied Clay Science*, **183**, 105331.

Yu W.B., Xu H.F., Tan D.Y., Fang Y.H., Roden E.E. & Wan Q. (2020) Adsorption of iodate on nanosized tubular halloysite. *Applied Clay Science*, **184**, 105407.

Zhang B.M., Han Z.X., Wang X.Q., Liu H.L., Wu H. & Feng H. (2019) Metal-bearing nanoparticles observed in soils and fault gouges over the Shenjiayao gold deposit and their significance. *Minerals*, **9**, 414.

Zhao J., Liu F.F., Wang Z.Y., Cao X.S. & Xing B.S. (2015) Heteroaggregation of graphene oxide with minerals in aqueous phase. *Environmental Science & Technology*, **49**, 2849–2857.

Zhou D.X., Abdel-Fattah A.I. & Keller A.A. (2012) Clay particles destabilize engineered nanoparticles in aqueous environments. *Environmental Science & Technology*, **46**, 7520–7526.

Zhou H.Y., Sun X.M., Cook N.J., Lin H., Fu Y., Zhong R.C. & Brugger J. (2017) Nano- to micron-scale particulate gold hosted by magnetite: a product of gold scavenging by bismuth melts. *Economic Geology*, **112**, 993–1010.

Zialame A., Jamshidi-Zanjani A. & Darban A.K. (2021) Stabilized magnetite nanoparticles for the remediation of arsenic contaminated soil. *Journal of Environmental Chemical Engineering*, **9**, 104821.